2822 *Inorg. Chem.* **2010**, *49*, 2822–2826
DOI: 10.1021/ic902222g

Inorganic Chemistry
Article

$MLi_2Ti_6O_{14}$ (M = Sr, Ba, 2Na) Lithium Insertion Titanate Materials: A Comparative Study

Damien Dambournet,* Ilias Belharouak,* and Khalil Amine

Chemical Sciences and Engineering Division, Argonne National Laboratory, 9700 South Cass Avenue, Argonne, Illinois 60439

Received November 10, 2009

$MLi_2Ti_6O_{14}$ (M = Sr, Ba, 2Na) titanates have been investigated as lithium insertion materials for lithium-ion batteries. A comparative study has been undertaken based on the structure, morphology, and electrochemical properties of the titanate materials, which were prepared by sol−gel synthesis. Their lithium insertion behavior was analyzed by crystallographic considerations. While $Na_2Li_2Ti_6O_{14}$ can reversibly host two Li^+ ions, $SrLi_2Ti_6O_{14}$ and $BaLi_2Ti_6O_{14}$ can reversibly insert almost four lithium ions per unit formula. Among the three materials, $SrLi_2Ti_6O_{14}$ showed superior capacity and rate capability. It was concluded that this class of materials could be of practical use in high-power lithium batteries for transportation applications.

Introduction

Lithium-ion batteries are being considered to power a new generation of clean vehicles. Battery life span, cost, and safety are still major barriers. With regard to safety, the issues associated with the formation of the solid−electrolyte interface (SEI) at the graphitic electrode can be overcome through the development of alternative anodes that can operate within the electrochemical stability zone of conventional electrolytes. This region is generally known to be above the potential (∼1 V) of the SEI formation and below the potential (∼4.3 V) of the electrolyte oxidation. The voltage profiles for tetravalent titanium-based materials such as $LiTi_2(PO_4)_3$,[1] TiO_2,[2] and $Li_4Ti_5O_{12}$[3] fall within this region. Their operating voltages are 2.5, 1.7, and 1.5 V, respectively, versus metallic lithium. Such a difference highlights the impact of the structural arrangement (i.e., the available sites, the neighboring atoms, and the ionocovalent character of the chemical bonds) on the energy of the Ti^{4+}/Ti^{3+} redox couple. It is therefore possible to tailor the energy of a given electrochemical couple based on the structure and the nature of the chemical bonding involved.[4] Recently, we investigated $MLi_2Ti_6O_{14}$ (M = Sr, Ba) materials as new lithium-ion insertion anodes.[5] These Ti^{4+}/Ti^{3+} electrodes showed lower operating voltage and lower resistivity compared to $Li_4Ti_5O_{12}$. More recently, the electrochemical properties of $Na_2Li_2Ti_6O_{14}$ were reported and found to possess even lower potential.[6] In the present paper, $MLi_2Ti_6O_{14}$ (M = Sr, Ba, 2Na) was investigated as an anode material based on structural and electrochemical characterization as well as crystallographic considerations.

Experimental Procedure

$MLi_2Ti_6O_{14}$ (M = Sr, Ba, 2Na) was synthesized by a sol−gel method. In a typical synthesis, lithium acetate hydrate with 5% stoichiometric excess and "M" acetate was mixed in a solution containing anhydrous ethanol and acetic acid with a volume ratio of 3.5. While the mixture was slightly heated, a stoichiometric amount of titanium isopropoxide was added, yielding a clear solution. The formed gel was heated at 200 °C overnight to complete the removal of the solvents. Finally, after grinding, the dry gel was annealed at 900 °C for 12 h under an air atmosphere.

Powder X-ray diffraction (XRD) analysis of the samples was performed with a Siemens D5000 diffractometer (Cu Kα). Scanning electron microscopy (SEM; Hitachi S-4700-II) was performed at the Electron Microscopy Center of Argonne National Laboratory.

Electrochemical measurements were carried out with CR2032-type coin cells. The $MLi_2Ti_6O_{14}$ electrodes were made of 80 wt % active materials, 10 wt % acetylene black as the conductive agent, and 10 wt % poly(vinylidene difluoride) as the binder. Copper was used as the current collector, and the area of the electrode was 1.6 cm^2. The electrolyte was 1.2 M $LiPF_6$ dissolved in a mixture of ethylene carbonate and ethyl methyl carbonate (3:7 volume ratio).

*To whom correspondence should be addressed. E-mail: dambournet@anl.gov (D.D.), belharouak@anl.gov (I.B.).

(1) Aatiq, A.; Ménétrier, M.; Croguennec, L.; Suard, E.; Delmas, C. *J. Mater. Chem.* **2002**, *12*, 2971.
(2) Murphy, D. W.; Cava, R. J.; Zahurak, S. M.; Santora, A. *Solid State Ionics* **1983**, *9&10*, 413.
(3) Ohzuku, T.; Aeda, A.; Yamamoto, N. *J. Electrochem. Soc.* **1995**, *142* (5), 1431.
(4) Goodenough, J. B.; Kim, Y. *Chem. Mater.* **2009**, DOI: 10.1021/cm901452z.
(5) Belharouak, I.; Amine, K. *Electrochem. Commun.* **2003**, *5*, 435.
(6) Yin, S. Y.; Song, L.; Wang, X. Y.; Huang, Y. H.; Zhang, K. L.; Zhang, Y. X. *Electrochem. Commun.* **2009**, *11*, 1251.

Published on Web 02/17/2010

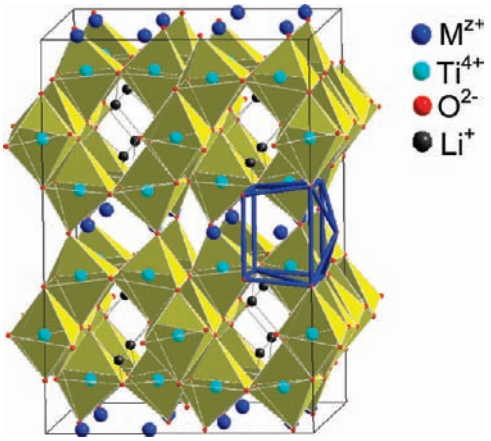

Figure 1. Schematic representation of the $MLi_2Ti_6O_{14}$ structure. The 11-fold-coordinated site highlighted by the blue edges is fully occupied, as displayed by the $Na_2Li_2Ti_6O_{14}$ structure.

The cells were assembled with lithium metal as the negative electrode and were tested in the voltage range of 0.5−2 V at different current densities. Cyclic voltammetry was performed with a Solartron analytical 1400 cell/test system over a potential of 0.5−2 V at a scan rate of 0.5 mV/s.

Results and Discussion

From a structural standpoint, the $MLi_2Ti_6O_{14}$ structure[7] is built upon edge- and corner-sharing TiO_6 octahedra, resulting in a three-dimensional network with voids suitable for lithium insertion (Figure 1). Within this structure, the lithium atoms are located in tetrahedral sites forming tunnels. The M atoms (M = Sr, Ba, 2Na) are 11-fold-coordinated and form a large and distorted cube (outlined in blue in Figure 1). The divalent cations Sr^{2+} and Ba^{2+} occupy half of the 11-fold-coordinated site, while sodium ions fully occupy this site. Therefore, $SrLi_2Ti_6O_{14}$ and $BaLi_2Ti_6O_{14}$ have more vacant sites available for lithium intercalation than $Na_2Li_2Ti_6O_{14}$ does. Another consequence of the total occupancy of the M site is an increase of the unit cell symmetry from the *Cmca* space group for strontium- and barium-based compounds to the *Fmmm* space group for $Na_2Li_2Ti_6O_{14}$.[8]

Figure 2 shows the XRD patterns of $MLi_2Ti_6O_{14}$. The unit cell parameters were calculated by using a profile-matching refinement (Table 1). The $BaLi_2Ti_6O_{14}$ and $Na_2Li_2Ti_6O_{14}$ compounds were found to be pure, while $SrLi_2Ti_6O_{14}$ exhibited a small peak at 27.4° (2θ), indicating unreacted TiO_2 rutile. This peak suggests that the formation of $SrLi_2Ti_6O_{14}$ requires higher temperature compared to the other samples.

The morphology of the prepared materials was determined by SEM (Figure 3). They were found to consist of submicrometer (~500 nm) primary particles that formed large agglomerates referred to as "secondary particles". Using the same synthesis protocol, we found the rate of particle agglomeration to be a function of the nature of the M ions in $MLi_2Ti_6O_{14}$. Indeed, the range of the secondary particle size evolved as follows: 1−5 μm for $Na_2Li_2Ti_6O_{14}$, 1−10 μm for $SrLi_2Ti_6O_{14}$, and 1−100 μm for $BaLi_2Ti_6O_{14}$. The effect of the morphology on the electrochemical properties of a material is well established, indicating that the existence of such large agglomerates in the case of $BaLi_2Ti_6O_{14}$ will reduce its overall capacity.

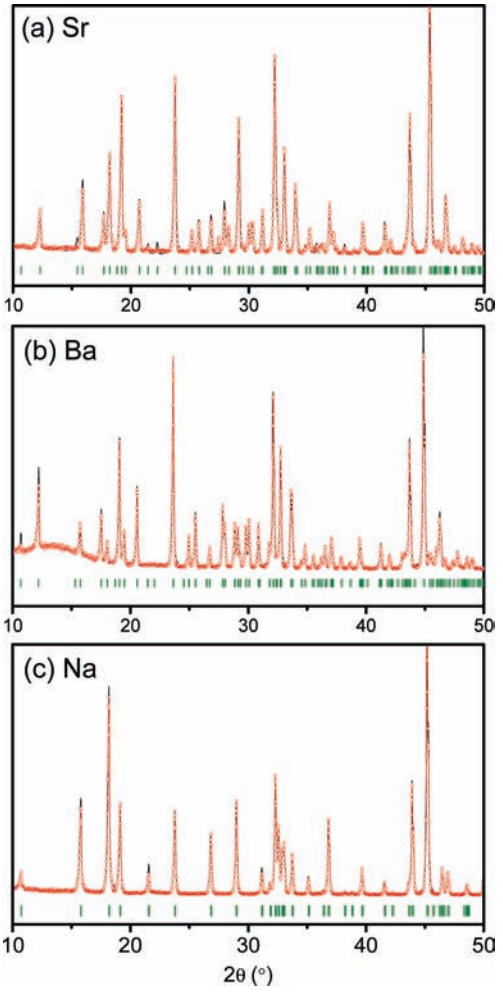

Figure 2. Profile matching of the powder XRD patterns of (a) $SrLi_2Ti_6O_{14}$, (b) $BaLi_2Ti_6O_{14}$, and (c) $Na_2Li_2Ti_6O_{14}$. Experimental and calculated diffractograms are in red and black, respectively; the Bragg positions are in green.

Table 1. Space Groups, Unit Cell Parameters, and Volumes of the $MLi_2Ti_6O_{14}$ Series

	Ba	Sr	Na
space group	*Cmca*	*Cmca*	*Fmmm*
unit cell parameters (Å)	a = 16.560(4)	a = 16.566(5)	a = 16.484(4)
	b = 11.257(3)	b = 11.139(3)	b = 5.737(1)
	c = 11.583(3)	c = 11.470(3)	c = 11.220(3)
volume (Å^3)	2159.25	2116.54	1061.06

Cyclic voltammetry measurements were carried out to characterize the electrochemical redox behavior of $MLi_2Ti_6O_{14}$ upon lithium-ion insertion and extraction. The cyclic voltammograms displayed in Figure 4 were obtained in the 0.5−2 V voltage range under a similar scan rate. In all cases, the reduction process that occurs at the electrodes during the initial cathodic sweep is different from those of subsequent cycles. Such a feature can be ascribed to local structural changes and/or to polarization of the cell. The observed peaks remain more or less constant starting from the second cathodic sweep. $SrLi_2Ti_6O_{14}$ and $BaLi_2Ti_6O_{14}$ compounds mainly exhibited an intense cathodic peak at 1.31 (Sr) and 1.27 V (Ba), in addition to a weak reduction peak at 1.0 V (Sr) and 1.07 V (Ba) (parts a and b of Figure 4, respectively).

(7) Koseva, I.; Chaminade, J. P.; Gravereau, P.; Pechev, S.; Peshev, P.; Etourneau, J. *J. Alloys Compd.* **2005**, *389*, 47.
(8) Nalbandyan, V. B. *Solid State Sci.* **2007**, *9*, 329.

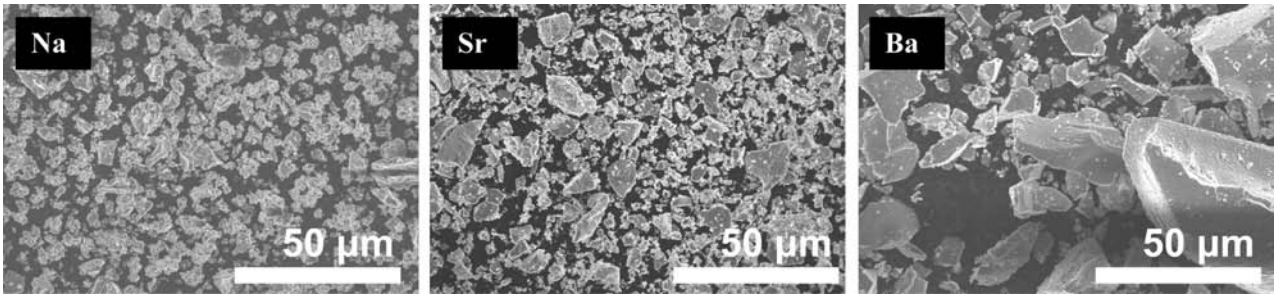

Figure 3. SEMs of $MLi_2Ti_6O_{14}$ prepared by sol−gel synthesis.

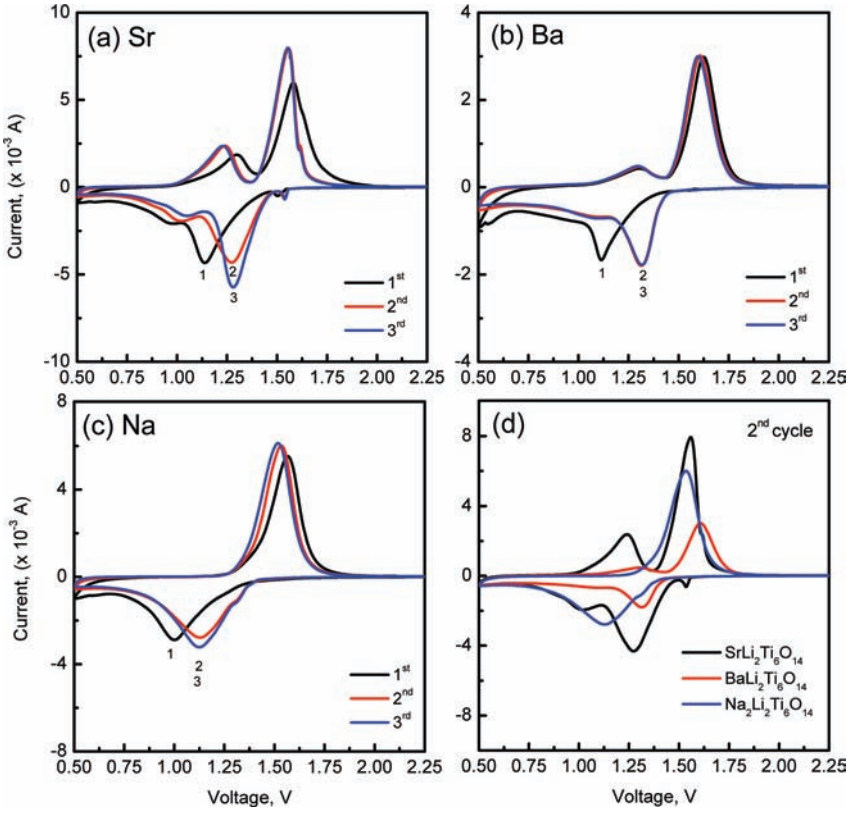

Figure 4. Cyclic voltammograms of (a) $SrLi_2Ti_6O_{14}$, (b) $BaLi_2Ti_6O_{14}$, and (c) $Na_2Li_2Ti_6O_{14}$ performed at 0.5 mV/s. (d) Second cycle of the three materials.

By contrast, $Na_2Li_2Ti_6O_{14}$ mainly showed a broad reduction peak at a potential of 1.12 V with a side shoulder at 1.3 V whose occurrence can be ascribed to the existence of different local lithium-ion insertion sites in the structure (Figure 4c). Note that the small reduction peak at 1.5 V for $SrLi_2Ti_6O_{14}$ (Figure 4a) is due to the existence of TiO_2 rutile in the compound. The anodic part of the voltammograms contained two peaks for $SrLi_2Ti_6O_{14}$ and $BaLi_2Ti_6O_{14}$ and one peak for $Na_2Li_2Ti_6O_{14}$, in good agreement with the number of cathodic peaks observed for these materials (Figure 4a−c). The results in Figure 4d clearly demonstrate that lithium-ion insertion occurs based on different mechanisms for these compounds, despite their apparent isostructural character.

The available vacant sites in $MLi_2Ti_6O_{14}$ (where M = Sr, Ba) were previously discussed in terms of the unoccupied Wyckoff positions within the *Cmca* space group.[5] Geometrical considerations based on interatomic distances suggested that the 8f, 8c, 4a, and 4b positions are suitable for hosting lithium ions (Table 2). The 8c, 4a, and 4b vacant sites are common sites for the three compounds (Table 2).

Table 2. Vacant Wyckoff Positions, Corresponding Atomic Positions, and Coordination Modes Based on the *Cmca* Space Group ($Z = 8$)

vacant Wyckoff position	atomic positions	coordination mode	availability in "M"$Li_2Ti_6O_{14}$
4a	0, 0, 0	4-fold	Na, Sr, Ba
4b	$^1/_2$, 0, 0	4-fold	Na, Sr, Ba
8c	$^1/_4$, $^1/_4$, 0	6-fold	Na, Sr, Ba
8f	0, x, y	11-fold	Sr, Ba

Considering the overall multiplicity ($Z = 8$), the total occupancy of these sites would lead to the insertion of two lithium ions per unit formula according to the following equation:

$$\square_{(8c,\,4a,\,4b)}MLi_2Ti_6O_{14} + 2e^- + 2Li^+ \leftrightarrow [Li_2]_{(8c,\,4a,\,4b)}MLi_2Ti_6O_{14}$$

The corresponding capacities should then be 87.5, 80, and 93.5 mAh/g for $SrLi_2Ti_6O_{14}$, $BaLi_2Ti_6O_{14}$, and $Na_2Li_2Ti_6O_{14}$, respectively.

Parts a−c of Figure 5 show typical voltage profiles for lithium cells made with $SrLi_2Ti_6O_{14}$, $BaLi_2Ti_6O_{14}$, and Na_2-

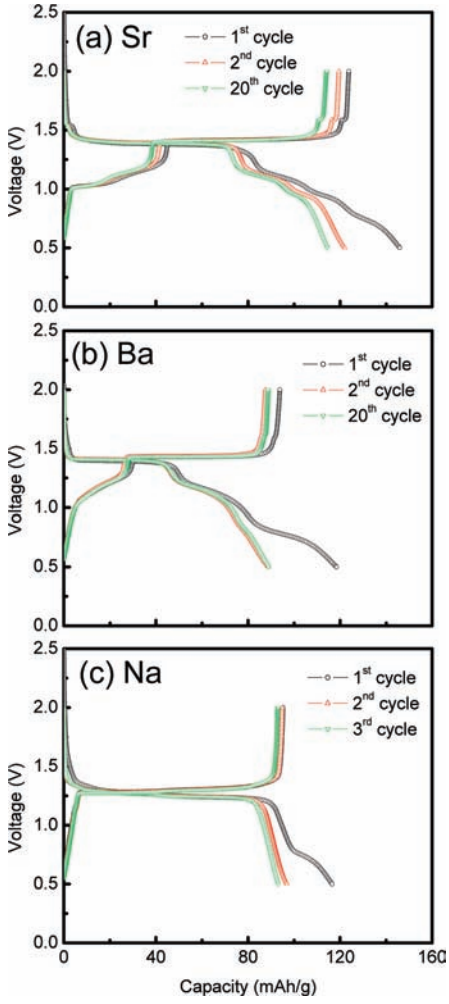

Figure 5. Charge/discharge voltage profiles of (a) $SrLi_2Ti_6O_{14}$, (b) $BaLi_2Ti_6O_{14}$, and (c) $Na_2Li_2Ti_6O_{14}$ cycled between 0.5 and 2 V at 10 mA/g.

$Li_2Ti_6O_{14}$ electrodes, respectively. The discharge and charge curves were recorded between 0.5 and 2 V under the same gravimetric current density of 10 mA/g. The initial discharge capacities were 145, 118, and 116 mAh/g for $SrLi_2Ti_6O_{14}$, $BaLi_2Ti_6O_{14}$, and $Na_2Li_2Ti_6O_{14}$, respectively. These numbers are higher than the capacities that were calculated based on the insertion of two Li^+ ions per unit formula. The observed capacities in Figure 5 can be broken down to capacities in the plateau regions, i.e., 80 mAh/g for $SrLi_2Ti_6O_{14}$ (1.4 V plateau), 48 mAh/g for $BaLi_2Ti_6O_{14}$ (1.4 V plateau), and 90 mAh/g for $Na_2Li_2Ti_6O_{14}$ (1.3 V plateau), along with additional capacities below the flat plateaus. Of these capacities, the values in the plateau regions approached the capacities that would be due to the insertion of two Li^+ ions in the cases of $SrLi_2Ti_6O_{14}$ and $Na_2Li_2Ti_6O_{14}$. However, because of its large particle size, a lower capacity was found for $BaLi_2Ti_6O_{14}$, i.e., 48 versus 80 mAh/g. $BaLi_2Ti_6O_{14}$ was then subjected to a high-speed ball milling to break down the large agglomerates (Figure 3c). XRD analysis revealed that the structure of this material is stable upon ball milling, and therefore further electrochemical tests were conducted. Figure 6 compares the voltage versus capacity profile of $BaLi_2Ti_6O_{14}$ before and after the ball-milling treatment. The ball-milled material delivered a capacity of 80 mAh/g in the first plateau region, in agreement with the insertion of

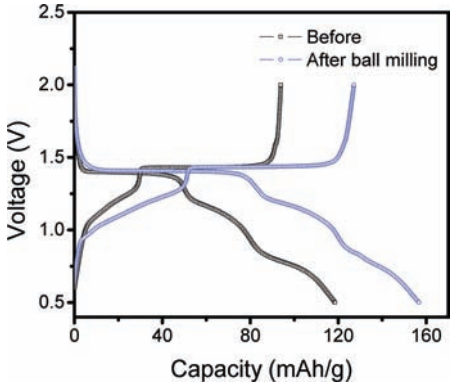

Figure 6. Charge/discharge voltage profiles of $BaLi_2Ti_6O_{14}$ cycled between 0.5 and 2 V at 10 mA/g, before and after the ball-milling treatment.

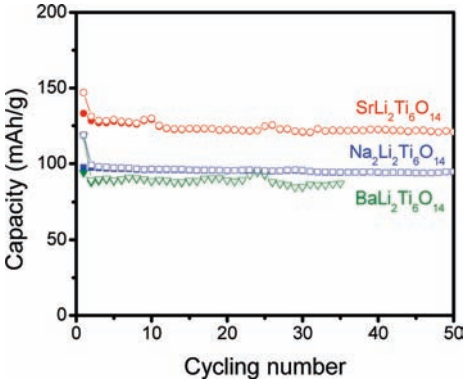

Figure 7. Voltage vs capacity profiles of the $MLi_2Ti_6O_{14}$ series cycled between 0.5 and 2 V at 10 mA/g.

two Li^+ ions in its structure per the above-proposed mechanism.

To explain the additional capacities that were observed below the plateau regions, a crystallographic approach was conducted in order to elucidate the existence of possible voids that are prone to lithium-ion insertion. Unlike $Na_2Li_2Ti_6O_{14}$, both $SrLi_2Ti_6O_{14}$ and $BaLi_2Ti_6O_{14}$ exhibit an additional vacant site 8f (Table 2), which is an 11-fold-coordinated space large enough to accommodate one or more Li^+ ions per unit formula (Figure 1, highlighted in blue). In a previous study,[5] discharge capacities obtained at a very low rate suggested reversible lithium uptakes of 3.55 and 3.8 Li^+ ions for $SrLi_2Ti_6O_{14}$ and $BaLi_2Ti_6O_{14}$, respectively. This finding suggests that the 8f vacant site in both materials can host up to two lithium ions in addition to the two Li^+ ions that are inserted during the plateau potential. Note that $Na_2Li_2Ti_6O_{14}$ can only host the last two Li^+ ions because Na^+ ions fully occupy the 8f site; this condition explains its lower overall capacity compared to those of $SrLi_2Ti_6O_{14}$ and $BaLi_2Ti_6O_{14}$. In all three materials, the capacity of the plateaus below 0.8 V was not reversible upon cycling. Ex-situ XRD performed at different states of charge did not show any significant change. While it confirmed the stability of the structure upon lithiation, it can not discriminate the origin of the observed irreversible capacity, arising from the electrolyte decomposition and/or irreversible lithium uptake.

In the following, the cycling stability and rate capability of the materials have been investigated. Figure 7 shows the cycling performance of $Li/MLi_2Ti_6O_{14}$ electrodes under 10 mA/g current density. After the first cycle, all electrodes

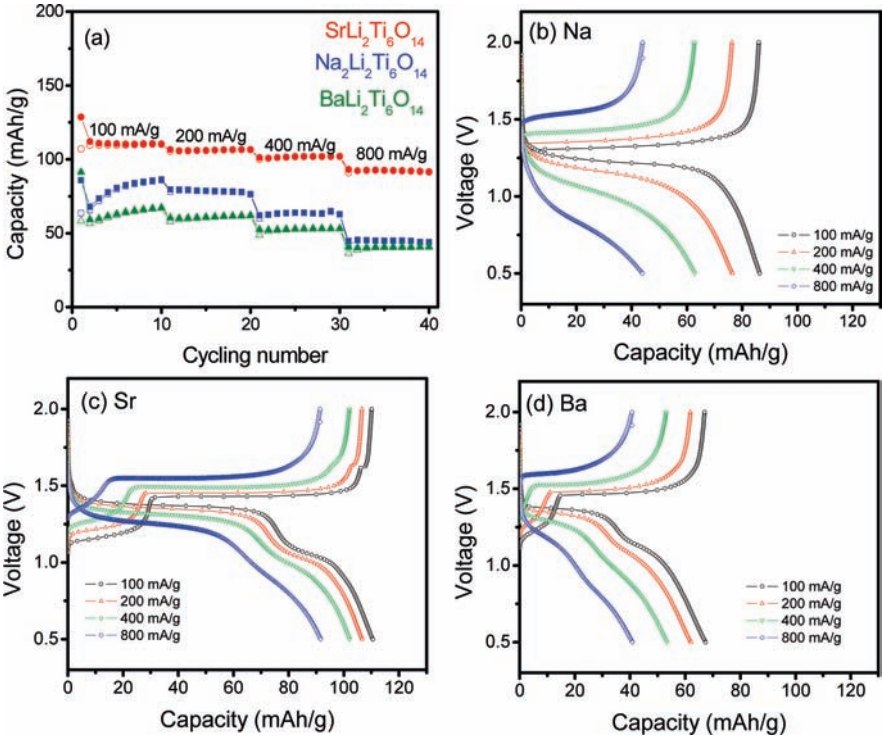

Figure 8. (a) Rate capability of $MLi_2Ti_6O_{14}$ tested between 0.5 and 2 V at 100, 200, 400, and 800 mA/g. Selected voltage profiles of (b) $Na_2Li_2Ti_6O_{14}$, (c) $SrLi_2Ti_6O_{14}$, and (d) $BaLi_2Ti_6O_{14}$ under different current densities.

exhibited stable cycling with high Coulombic efficiencies. The $SrLi_2Ti_6O_{14}$ and $Na_2Li_2Ti_6O_{14}$ electrodes delivered 120 and 95 mAh/g over 50 cycles. $BaLi_2Ti_6O_{14}$ delivered a lower capacity because of its large particle size, but the ball-milling treatment resulted in 120 mAh/g capacity over 50 cycles, the same as that found for $SrLi_2Ti_6O_{14}$. Figure 8a shows the rate capability versus the cycle number of the three materials cycled under increasing current densities of 100, 200, 400, and 800 mA/g. The $SrLi_2Ti_6O_{14}$ electrode showed superior rate capability and less polarization compared to the other materials (Figure 8b−d). Indeed, this material was able to deliver and sustain 92 mAh/g capacity under 15 min of discharge and charge conditions, i.e., 800 mA/g current density. This result suggests that $SrLi_2Ti_6O_{14}$ is a promising anode material for high-power lithium-ion batteries for transportation applications. Furthermore, multiple ways are available to improve its electrochemical properties, such as particle size reduction and surface modifications. Finally, this material is suitable to be combined with high-power cathodes such as a $LiMn_2O_4$ spinel.

Conclusion

The $MLi_2Ti_6O_{14}$ (M = Sr, Ba, 2Na) series has been synthesized by a sol−gel method. The three compounds are isostructural, exhibiting open channels and enabling the reversible insertion of lithium ions. The materials possess common vacant sites (namely, 8c, 4a, and 4b of the *Cmca* space group) and can accept two lithium ions per unit formula, leading to a plateau region in their voltage versus capacity profiles. The structure of $Na_2Li_2Ti_6O_{14}$ slightly differs from those of $SrLi_2Ti_6O_{14}$ and $BaLi_2Ti_6O_{14}$ because sodium ions fully occupy the 11-fold-coordinated site displayed by its framework. Therefore, $Na_2Li_2Ti_6O_{14}$ cannot host more than two Li^+ ions per unit formula, which corresponds to 95 mAh/g capacity. The vacant 8f sites available in the $SrLi_2Ti_6O_{14}$ and $BaLi_2Ti_6O_{14}$ structures enabled the uptake of additional Li^+ ions, i.e., 1.5−2 Li^+ ions per unit formula, leading to superior capacities compared to that of $Na_2Li_2Ti_6O_{14}$, as confirmed by cyclic voltammetry and galvanostatic measurements. Except for $BaLi_2Ti_6O_{14}$, where the existence of large agglomerates blocked the achievement of full capacity, the other materials exhibited capacities close to theoretical. Of these materials, $SrLi_2Ti_6O_{14}$ showed superior electrochemical properties: a capacity of 120 mAh/g over 50 cycles under the C/14 rate and 92 mAh/g under the 4C rate. This class of materials is therefore suggested to be promising anodes in high-power lithium-ion batteries.

Acknowledgment. This research was funded by the U.S. Department of Energy, FreedomCAR, and Vehicle Technologies Office. Argonne National Laboratory is operated for the U.S. Department of Energy by UChicago Argonne, LLC, under Contract DE-ACO2-06CH11357.